Double-containment coil with enhanced winding mounting for transcranial magnetic stimulation with reduced acoustic noise

Supplementary material

Lari M. Koponen, Stefan M. Goetz, Angel V. Peterchev

Double containment coil for ultra-brief TMS pulses

In this supplementary material, we present an alternative version of the winding block (WB) for our double containment coil (DCC). In the main text we refer to this version of the coil as DCC*. Instead of solid magnet wire, this alternative WB is wound with litz wire, which ensures compatibility with ultra-brief TMS pulses with much higher characteristic frequency.

In ultra-brief TMS pulses, the total duration of the biphasic pulse will be reduced by an order of magnitude, from 300 µs down to about 30 µs (Peterchev et al., 2015). To induce super-threshold stimulation, these ultra-brief pulses are expected to require approximately ten times higher E-field amplitude than conventional pulses, and consequently require comparable peak coil current. This necessitates next-generation TMS devices with operating voltages of approximately 10 kV (Peterchev et al., 2015). The main benefit of ultra-brief pulses is that they are expected to further reduce the sound level by both pushing the spectral peak at two times the pulse current frequency outside the human hearing range and by reducing the energy in the excited subharmonics by a factor of 10. Given that the DCC containment provides its best attenuation at high frequencies, its combination with ultra-brief pulses may further reduce both SPL and SL by more than 20 dB for a truly quiet TMS device.

To be compatible with ultra-brief, high-voltage pulses, we wound the alternative WB from a 4.06 mm × 2.08 mm rectangular litz wire (120 strands of 0.2 mm enameled copper wire, total copper cross section of 3.84 mm^2) wrapped in three layers of 25 µm polyimide film (New England Wire, USA). This WB is shown in Fig. S1.

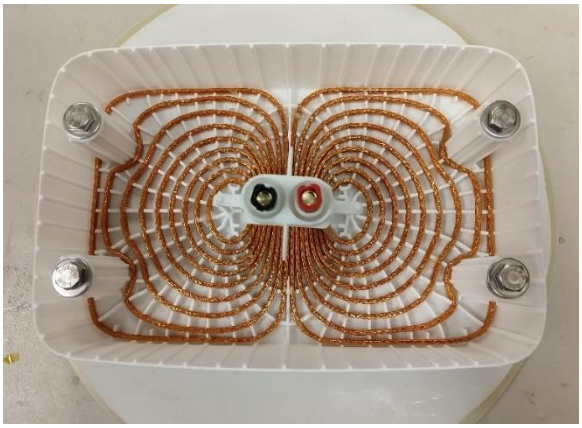

Fig. S1. Winding block (WB) otherwise identical to that of Fig. 2 but wound with high-voltage litz wire for DCC*.

As this litz wire has lower copper cross section than the solid magnet wire in the work, it has higher dc resistance. Consequently, the simulated coil inductance and resistance for the litz-wire WB were, respectively, 11.0 µH (10.8 µH for the coil winding and 0.15 µH for the power cable) and 25.3 mΩ (20.0 mΩ for the winding and 5.3 mΩ for the cable). These values matched very well the respective measurements of 11.7 µH and 29.0 mΩ at 1 kHz, and 11.7 µH and 28.2 mΩ at 10 kHz, acquired with B&K Precision Model 889A Bench LCR/ESR Meter (B&K Precision Corporation, USA). As with the solid-wire WB, the unaccounted inductance and resistance likely stem from parasitic inductance and resistance associated with the connections between the winding, coil cable, and measurement probe.

The simulated coupling coefficient to cortex was 1.42 (V/m)/(A/µs) for the entire coil, and 1.67 (V/m)/(A/µs) for the exposed coil WB, virtually identical to the solid-wire WB. When connected to the MagPro TMS device, the pulse duration for biphasic TMS pulses was 293 µs, which was close to conventional MagVenture coils. The measured coupling coefficients were 1.42 (V/m)/(A/µs) for the coil, and 1.68 (V/m)/(A/µs) for the exposed WB, matching the simulations. When powered with the same MagVenture TMS device, compared to the solid-wire WB, the litz-wire WB had 1.2% lower E-field, most likely due to manufacturing tolerances with the windings. The maximum stimulation strength, however, was 4.5% lower. The latter was due to more resistive losses during the pulse, and therefore more damping of the sinusoidal biphasic waveform. Consequently, the stimulation strength at 100% of maximum stimulator output (MSO) was 262% and 310% of average RMT for the entire coil and the exposed WB, respectively.

The litz-wire WB was slightly louder than the solid-wire WB and had notably larger peak SPL (compare Fig. S2 to Fig. 4 in the main text). This additional loudness of the litz-wire WB and DCC*, stems from increased amount of high-frequency content in the sound. This is likely due to the less rigid WB, which can be seen in the simulations at the top of Fig. S3 and from the comparison to the solid-wire DCC in Fig. S4. The difference between the solid-wire and litz-wire WB is, however, much smaller than the expected sound reduction from ultra-brief pulses. Further, the outer casing greatly reduced the difference in SL.

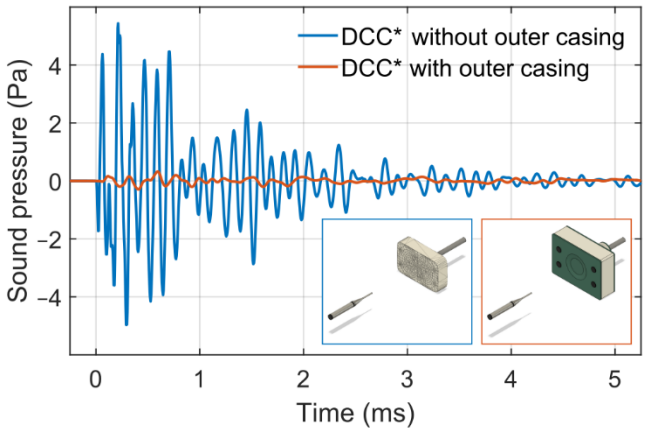

Fig. S2. Sound pressure waveforms from the litz-wire coil prototype (DCC*) and its WB. In both cases, the microphone was centered 25 cm from the closest head-facing surface (insets). The start of the TMS pulses is at –0.73 ms to compensate for the sound propagation delay in the air. The exposed WB (109 dB(Z) peak) is compared to the complete coil with outer casing (84 dB(Z) peak). Both configurations are measured for stimulation strength of 167% RMT; thus, the complete coil had 18% higher current to compensate for the thickness of the casing.

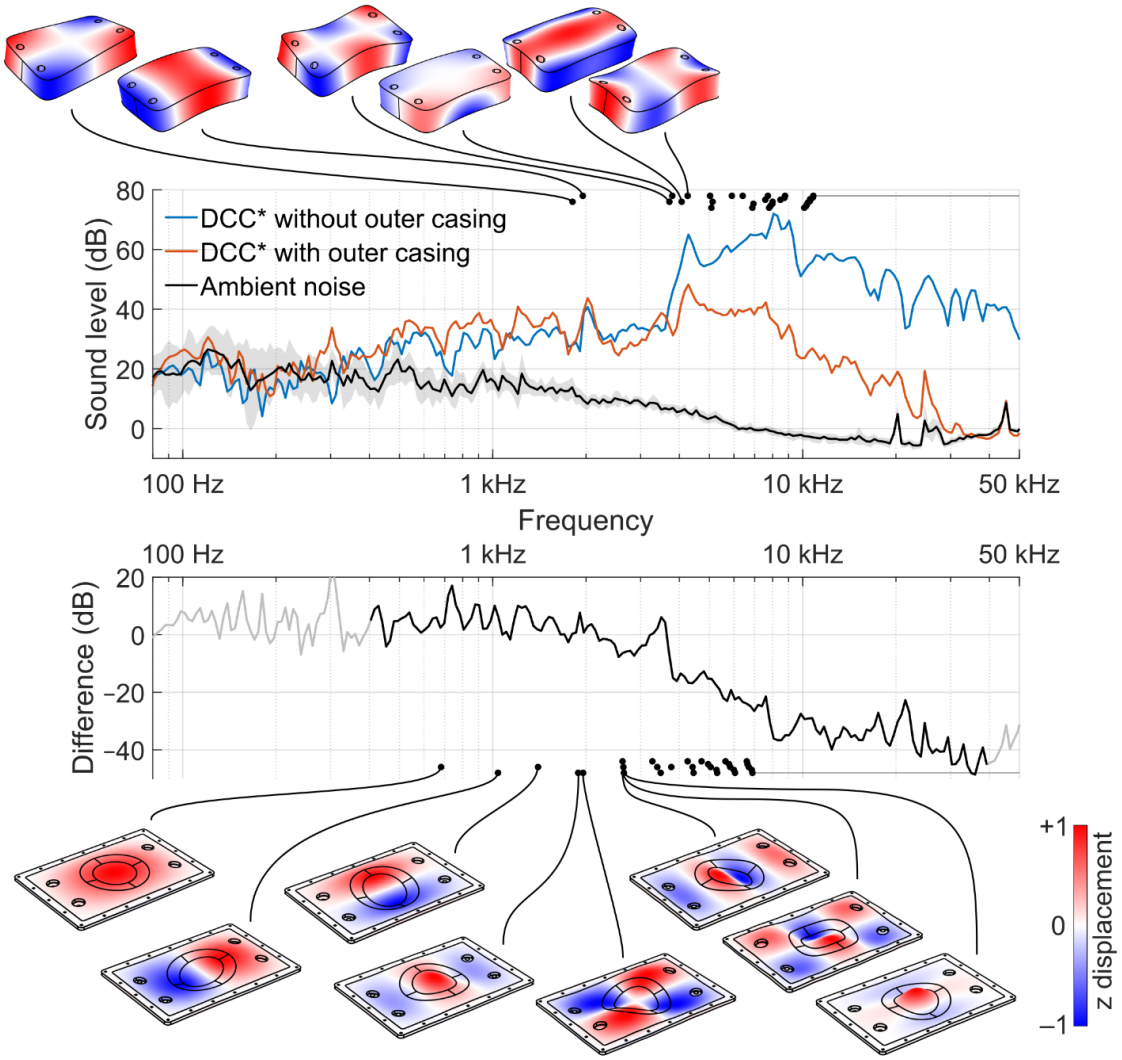

Fig. S3. Measured sound spectra and simulated mechanical vibration modes of the prototype litz-wire DCC*. Similar to Fig. 3, except for lack of laser Doppler vibrometer (LDV) measurements. The measured sound spectra plots in dB are compared with the simulated mechanical modes, illustrated with surface displacement plots, black dots denoting the resonant frequencies, and black lines connecting them. Top: Six lowest WB vibration modes. Second row: 1/24-octave sound level of the WB and complete coil with outer casing at 167% average resting motor threshold (RMT). To reduce the ambient noise level, 9 pulses were averaged for each trace. The gray band denotes the 95% confidence interval of the averaged ambient noise measurement. Third row: Attenuation provided by the outer casing obtained by subtracting the WB spectrum from the complete coil spectrum. Despite averaging, the attenuation spectrum at frequencies below 400 Hz and above 40,000 Hz could not be measured reliably and is therefore grayed out. Bottom: Vibration modes of the outer casing lid.

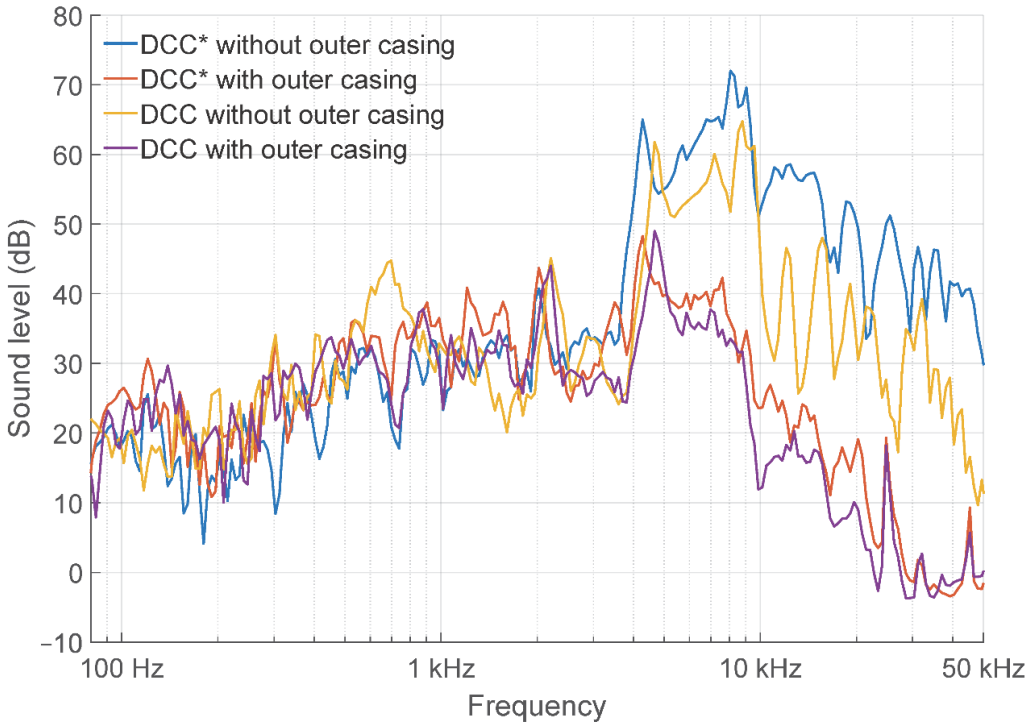

Fig. S4. Comparison of the sound spectra of the litz-wire DCC* and the solid-wire DCC. The primary difference is in measurements of the WB without the outer casing, where the litz-wire WB has larger high-frequency components. The outer casing reduces the difference between the two WBs but does not entirely eliminate it.

Estimation of peak sound pressure level (SPL) at coil surface

In the main part of this work, we measured the sound at 25 cm from the TMS coil and extrapolated the sound pressure level and sound level at 5 cm from these data. This method avoids two issues related to measuring very close to the TMS coil. First, we can separate the sound and the TMS-induced artefact in the microphones as they are separated in time due to the limited speed of sound. Second, at 25 cm a single measurement point will capture sound originating from any point of the head-facing side of the coil, and we avoid most problems associated with spatial undersampling of the sound.

Ideally, we would like to validate such extrapolation for coils such as DCC which are much larger than 5 cm in size. An approximate validation is possible with the laser Doppler vibrometer (LDV) data. A TMS coil is a pressure source for sound. Consequently, for small surface vibrations

$$p(\boldsymbol{x},t) = \frac{\rho}{2\pi}\iint_S \frac{a\left(\boldsymbol{x}', t-\frac{R}{c}\right)}{R}\,dS' \qquad (1)$$

where $p(\boldsymbol{x},t)$ is the sound pressure at location $\boldsymbol{x}$ at time t; ρ is the density of air; $a(\boldsymbol{x}',t')$ is the normal component of the coil surface acceleration at location $\boldsymbol{x}'$ at retarded time $t' = t - R/c$, where R is the distance between the two locations and c is the speed of sound in air; and S is the coil surface (Pierce, 2019). This equation assumes that the coil surface is a part of an infinite plane, i.e., it omits diffraction due to edges of the coil, and for the DCC it omits any directional effects due to the center recession in the lid.

To avoid undersampling, we must perform relatively dense spatial sampling of the coil surface to avoid missing potential loud spots. The 41 points used for the LDV measurements of the DCC lid were likely sufficient as the sound varies smoothly from one point to its neighbors (Fig. S5, left). However, the equally dense 25 point grid for the WB potentially failed to find the loudest spot on the WB surface as the sound varies considerably between neighboring points (Fig. S5, right). Nonetheless, we carried out the integration of Eq. 1 with a simple zeroth order quadrature for both the lid and WB measurements. Each sample point gets a surface weight of its area in the Voronoi diagram of the sampling points. With this quadrature, we obtain a reasonable reproduction of the measured sound at 25 cm (Fig. S6), and most importantly we confirm that the simple extrapolation of the peak SPL produces reasonable prediction errors down to 3 cm for both the DCC and its WB without the outer casing (Fig. S6).

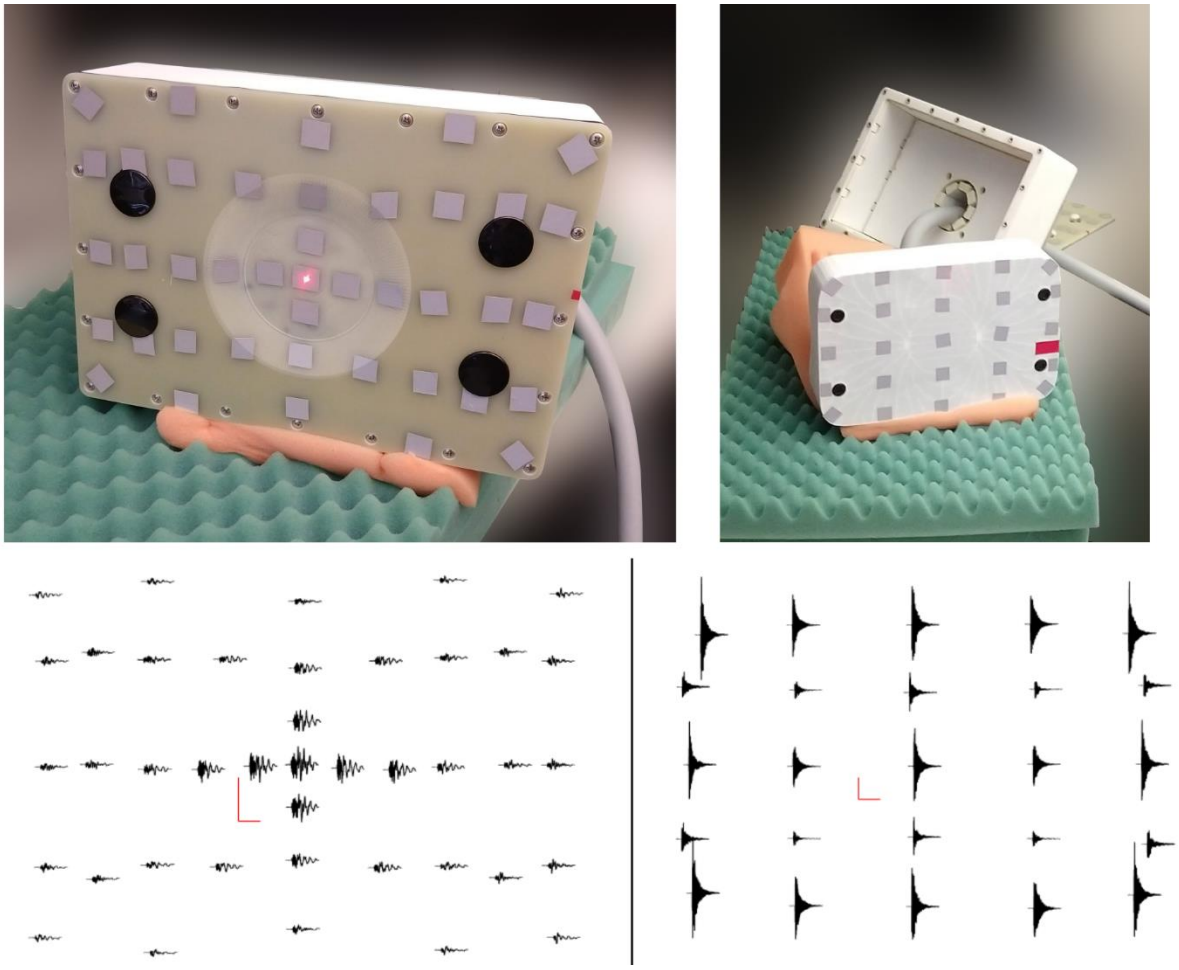

Fig. S5. LDV measurements of the vibration velocity distribution on the surfaces of the DCC lid (left) and the WB (right). All points were measured at 50% MSO. The red horizontal and vertical scale bars are 10 ms and 10 mm/s, respectively.

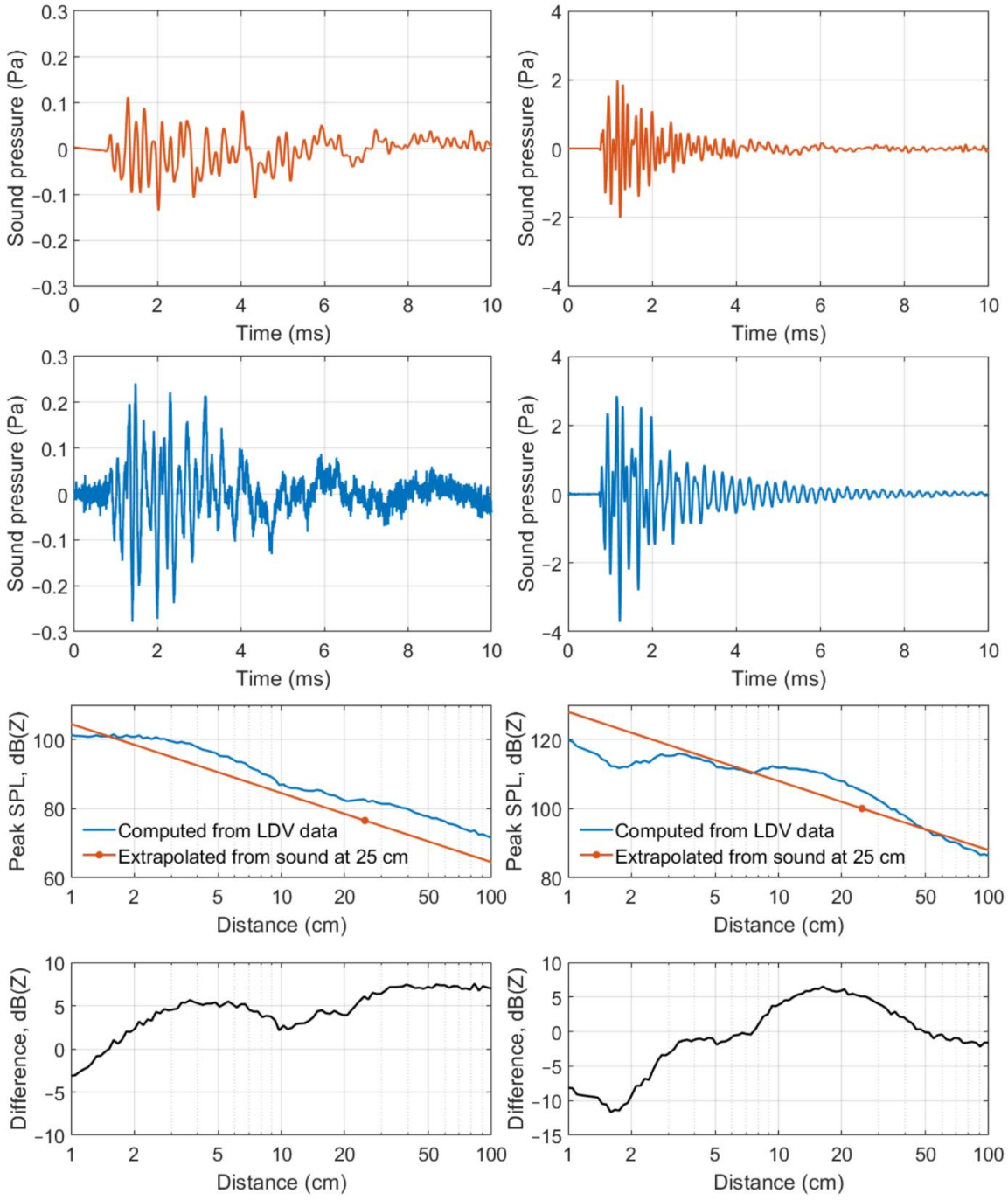

Fig. S6. Comparison of LDV and microphone measurements of the SPL of the DCC (left) and its WB (right). First row: Sound waveform measured with microphone at 25 cm from the surface. DCC and WB have peak SPL of 76.6 and 100.1 dB(Z), respectively. Second row: Sound waveform computed from the LDV data for distance of 25 cm from the surface. This computation slightly overestimates both, at 82.9 and 105.4 dB(Z), respectively. The error is predominantly in the amplitude of individual oscillations of the high-frequency component of the sound. Third row: Peak SPL as a function of distance from the surface, computed from the LDV data and extrapolated from the microphone measurement at 25 cm. Fourth row: Difference between the two estimates in the third row.

References

A. V. Peterchev *et al.*, “Quiet transcranial magnetic stimulation: status and future directions,” in *2015 37th Annual International Conference of the IEEE Engineering in Medicine and Biology Society (EMBC)*, Aug. 2015, pp. 226–229, doi: 10.1109/EMBC.2015.7318341.

A. D. Pierce, Acoustics: An Introduction to Its Physical Principles and Applications, 3rd ed. Cham, Switzerland: Springer, 2019.